Journal of Polymers and the Environment
https://doi.org/10.1007/s10924-022-02740-7

ORIGINAL PAPER

Ionic Liquid/ZnO Assisted Preparation of High Barrier Cellulose Nanocomposite Films by In Situ Ring-Opening Polymerization of Lactide Monomers

Elahe Amini[1] · Cristina Valls[1] · Hossein Yousefi[2] · M. Blanca Roncero[1]

Accepted: 9 December 2022

Abstract
Cellulose-based composites have aroused increasing interest as potential replacements for fossil fuel-based plastics. In this work, transparent cellulose-grafted-PLA nanocomposite films were prepared by grafting polylactide (PLA) onto cellulose. PLA was synthesized by in situ ring opening polymerization from a regenerated cellulose matrix, using zinc oxide nanoparticles (ZnONPs) in 1-ethyl-3-methylimidazolium acetate (EmimAc) as solvent. A facile route was devised to modify the starting material (cellulose paper) by partial dissolution and regeneration that used an ionic liquid (IL) as a smart nanowelding agent to assemble nanometric cellulose structures. The influence of the proportion of ZnONPs (1–5 wt%) and *L*-lactide (LA) monomers (10–70 wt%) used on the properties of the resulting nanocomposite films was examined by comparison with an all-cellulose composite (ACC) and pure cellulose paper. Incorporating ZnONPs and PLA was found to enhance the mechanical, barrier and optical properties of the films. The maximum tensile strength and best barrier properties were those of a film obtained from 5%ZnONPs and 70%LA. FTIR spectra confirmed a new form of interaction between PLA and the regenerated cellulose matrix. Also, XRD spectra revealed a transition from cellulose I to II and an increase in the proportion of noncrystalline cellulose through partial dissolution and regeneration. Although the surface morphology of the nanocomposite films was influenced by the presence of ZnONPs and PLA chains, their color and chemical structure were not. The transparent cellulose-grafted-PLA nanocomposite films obtained are highly promising as packaging materials.

Keywords Transparent nanocomposite film · Ionic liquid · ZnO nanoparticles · Partial dissolution · Direct nanowelding · Ring opening polymerization · PLA

Introduction

In recent years, environmental concerns and the demand for biorenewable polymers have aroused increasing interest in designing multifunctional biocomposites. Unlike nondegradable polymers and polymeric composites, biocomposites are easily biodegraded [1]. Cellulose is widely used as a matrix or reinforcing material for biocomposites on the grounds of its biocompatibility, biodegradability, recyclability, nontoxicity and low cost, among other properties [2]. Also, cellulose resists dissolution in most common solvents thanks to its highly stiff hydrogen bond network and partially crystalline structure [3]. As can be seen in Fig. 1, cellulose fibers typically exhibit micro-disconnections or gaps (lumens and pits) and nano-disconnections (e.g., gaps along adjacent nanofibrils). As a result, increasing cellulose accessibility entails disrupting fibril aggregates and highly ordered regions [4]. This should ideally accomplished by using a simple, efficient, environmentally friendly method to avoid massive disruption of the native structure [5].

Nanowelding is a novel process for modifying cellulose fibers at the nanometric scale that enables direct production of high-quality cellulose nanocomposites with tailored structural and physical properties, functions and uses [6, 7]. The idea behind direct nanowelding of cellulose fibers is that a solvent can penetrate deeply into their nanostructure by creating a disordered phase and partially dissolving the

✉ Elahe Amini
elahe.amini@upc.edu

[1] CELBIOTECH_Paper Engineering Research Group, Universitat Politècnica de Catalunya (UPC), Colom 11, 08222 Terrassa, Barcelona, Spain

[2] Wood Engineering and Technology, Gorgan University of Agricultural Sciences and Natural Resources, Gorgan, Iran

Published online: 03 January 2023

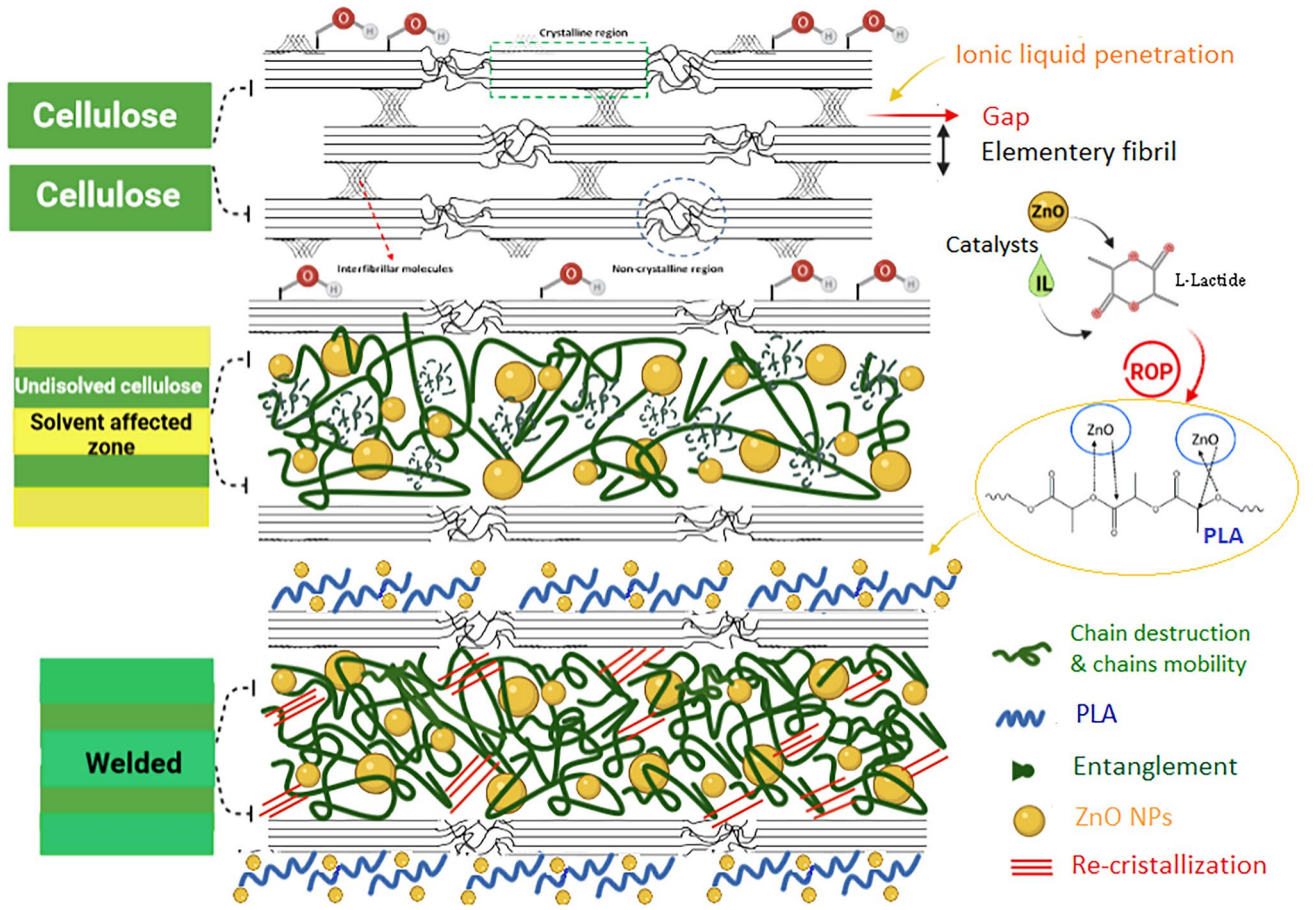

Fig. 1 Schematic depiction of the grafting of PLA polymers onto cellulose fibers to form a cellulose-grafted nanocomposite film with entrapped ZnONPs in its micro- and nanosized structures

skin part of cellulose Iβ. During the dissolution-regeneration process, the skin dissolved region becomes a welded layer between nanofibrils [5, 6]. The procedure potentially allows various types of nanomaterials to be added during cellulose dissolution in order to obtain nanocomposites with specific properties. Yousefi et al. [6, 8] investigated the role of nanojoining in the partial dissolution of cellulose by using an ionic liquid to obtain all-cellulose composites (ACCs). ACCs are a new type of self-reinforced (single-component) composites in which cellulose acts as both the matrix and the reinforcing material. ACCs can be obtained in two main ways. One is a single-step method that involves partial dissolution of cellulose and in situ regeneration of the dissolved portion as matrix around the undissolved portion as reinforcement. The other is a two-step method in which cellulose is partially dissolved and then regenerated in the presence of undissolved cellulose, which allows the regenerated and undissolved cellulose fractions to be obtained from different natural sources [9, 10].

Ionic liquids (ILs) are a class of green solvents with a number of attractive advantages including a low melting point (< 100 °C), high thermal stability, lack of volatile components, nonflammability, miscibility with many solvent systems and the ability to easily dissolve cellulose fibers [10]. These unique properties have enabled their widespread use as reaction media and as catalysts in polymerization [11]. In addition, ILs are scarcely prone to decomposing polymer matrices during processing [7]. Previous work by Niu et al. [5] on the use of ILs as welding agents showed their ability to swell the compact structure of cellulose fibers by creating disordered cellulose domains on the surface of nanosized fibrils, connecting them together and forming a continuous integrated network. In addition, the dissolution-regeneration process reduced crystallinity or resulted in conversion to cellulose II. Imidazolium based ILs such as 1-ethyl-3-methylimidazolium acetate (EmimAc) can be used as reaction media for interaction with cellulose fibers thanks to their low dissolution temperature and modest energy requirements. Also, residual EmimAc potentially retained by cellulose fibers after washing is nontoxic [12, 13].

Graft polymerization with cyclic esters or reinforcement with other polymers can provide an impressive route to develop environmentally adaptable, biocompatible cellulose-based materials for a number of futuristic uses [14, 15]. Cellulose grafted copolymers, where side chains are bonded to the cellulose backbone, are highly useful materials combining the benefits of natural cellulose and the functionalities of grafted polymers [16, 17]. Poly(lactide) (PLA) has been deemed the most promising bioplastic material on the grounds of its excellent properties and vast range of potential uses [18]. In fact, PLA is biodegradable, biocompatible, recyclable, eco-friendly, economical and virtually nontoxic; also, it possesses excellent thermal strength and superior transparency properties, and can be readily obtained in various forms [19, 20]. Despite its advantages, the use of PLA in packaging, automotive and biomedical materialsis limited by its brittleness; low degree of crystallization; and poor toughness, gas barrier and thermal properties relative to conventional thermoplastic [19, 21]. These shortcomings can to some extent be circumvented by combining it with cellulose through in situ polymerization of *L*-lactide monomers.

Ring opening polymerization (ROP) is a form of chain-growth polymerization that involves cleavage of rings in cyclic monomers such as or lactides to facilitate the formation of polymers. This could provide an effective route to modify polysaccharides [22]. Hydroxyl groups in cellulose often act as initiators in the ROP of cyclic monomers for modification of cellulose or its derivatives [23]. Hafren and Cordova [24, 25] reported the first surface-initiated ROP of a cellulose substrate with the need for no chemical treatment of the cellulose prior to grafting. They successfully grafted ϵ-caprolactone from cellulose paper by using organic or amino acids as catalysts. FTIR spectra exhibited a peak at 1730 cm^{-1} that was assigned to the carbonyl group in polycaprolactone. These authors also succeeded in polymerizing LA from the cellulose surface by using tartaric acid in the absence of a catalyst [24, 25]. Yan et al. [26] and Dong et al. [27] synthesized cellulose-grafted-PLA copolymers in the ionic liquid 1-allyl-3-methylimidazolium chloride with stannous octoate $Sn(Oct)_2$ and 4-dimethylaminopyridine, respectively, as catalyst.

Nanoparticles have attracted much attention in recent years by virtue of their excellent properties for different uses including food packaging, biodegradable materials, electronic devices, optics, sensors, and biomedical and catalysis science [28]. Specifically, ZnO nanoparticles (ZnONPs) have aroused enormous interest from their great unique properties, which include excellent biocompatibility, intrinsic nontoxicity, low cost, UV-shielding efficiency and antibacterial activity [29]. It would be especially interesting to create films with UV barrier properties to prevent or delay oxidation of food components and preserve them throughout storage and transit to ensure that they retain their nutritional value [30]. Facile syntheses of multifunctional materials in one step are gaining importance in this context. Thus, Kaur et al. [31] and Rodriguez-Tobias et al. [32] successfully prepared PLA/ZnO nanocomposites by ROP of *L*-lactide monomer in the presence of ZnONPs, ZnO itself acting as the catalyst. The preparation procedure is environmentally benign [31, 32]. One major drawback of ZnONPs is their tendency to agglomerate and aggregate, which reduces the efficiency of the resulting nanomaterials. This problem can be alleviated by using an appropriate ionic liquid as dispersion medium. Thus, ILs provide electrostatic protection by forming a "protective shell" onto metal nanoparticles that are thus rendered stable without the need for additional stabilizers, surfactants or covering ligands [33].

In this work, we used ZnONPs and an IL as catalysts for the ring-opening polymerization of *L*-lactide to synthesize cellulose-grafted-PLA nanocomposites in one step. The ionic liquid was used as a smart nanowelding agent to assemble nanometric cellulose structures with the partial dissolution method. The nanoparticles and IL were used not only for ROP of *L*-lactide monomers from the skeleton of cellulose as backbone but also to facilitate multifunctional uses of the resulting transparent nanocomposite films (Fig. 1). The role of each component of the film was investigated with a view to optimizing water and oxygen barrier properties, strength and UV-blocking capacity. As shown by the results, the films can be used as packaging materials.

Materials and Methods

Materials

The highly purified bleached fibers of cotton linter pulp was provided by Celsur, Spain. 1-Ethyl-3-methylimidazolium acetate (analytical reagent grade, 98%), and ZnO dispersion (40 nm average particle size, 20 wt% in H_2O), were supplied by Sigma-Aldrich. *L*-lactide (LA) was obtained from Panreac Química SLU Co., Spain. Other chemicals were used as analytical reagents without further purification.

Preparation of the Original All-Cellulose Paper

The purified cotton linter pulp with more than 90% α-cellulose content was used for the preparation of original paper. The α-cellulose content was calculated by TAPPI T203. The paper formation machine (Rapid-Köthen method) was used for getting the original paper according to ISO 5269-2. Then the wet paper was blotted between two stacks of regular filter paper, which pressed under a pressure of 0.1 MPa and dried at 90 °C for 10 min.

Preparation of Cellulose-Grafted-PLA Nanocomposite and All-Cellulose Composite Film

After performing several experimental tests, the method of preparing transparent cellulose-grafted-PLA nanocomposite film is briefly described as below. The starting orginal all-cellulose paper, IL, and the glassware are dried to avoid any negative effect of water on the dissolution of cellulose. 3 ml ionic liquid solution was firstly mixed with different contents of LA (10, 30, 50, 70%, w/w, original paper) and ZnO nanoparticles (1, 3, 5%, w/w, original paper). To improve the grafting efficiency, the mixture was then stirred at 700 rpm for 30 min at 80 °C temperature to initiate ring-opening polymerization of LA monomers. After making the ROP and nanowelding solution, the dried original paper (25 mg with thickness: 122 × 4.08 µm) with grammage of 40 g/m^2 and an area of 64 cm^2 was placed into a glass petri dish. After that, the solution was added onto the surface of the paper. For IL-assisted in situ ROP of LA in the presence of ZnO nanoparticles and partial dissolution of cellulose, the process was allowed to proceed in an oven at 80 °C for 24 h. At the end of the dissolution time, the gel film was removed from the oven and allowed to cool at the room temperature. Afterwards, the gel film was washed by coagulation in deionized water and a transparent nanocomposite gel resulted. To eliminate residual ionic liquid in the regenerated sample, the gel was washed several times. After that, the obtained nanocomposite film was sandwiched between two glass plates and oven-dried at 60 °C for 1 h. Finally, the wet nanocomposite was blotted between filter paper and a glass plate to dry at 50% relative humidity (RH) and 25 °C for at least 3 days. Finally, nanocomposite films were obtained with a thickness of 49–62 µm. The thicknesses of nanocomposite films are summarized in Table 2. The all-cellulose composite film as control sample with thickness of 48 × 2.05 µm was obtained using the above mentioned method without using ZnONPs and grafting PLA polymer chains.

Characterization

Degree of Polymerization (DP) of Cellulose

The limiting viscosity number in cupriethylenediamine (CED) solution was used for determining the viscosity index of cellulose in the cotton linter pulp, ACC and cellulose-grafted-PLA nanocomposite films according to ISO 5351 standard, using a capillary viscometer. The Mark–Houwink–Sakurada equation was used to calculate average DP.

Estimation of Grafting Parameters

Grafting parameters such as % grafting, % grafting efficiency and % homopolymer were calculated gravimetrically using the following equations (1)-(3), respectively [34]:

$$Percent\ grafting\ (\%G) = \frac{(W_1 - W_o)}{W_o} \times 100 \quad (1)$$

$$Percent\ grafting\ efficiency\ (\%GE) = \frac{(W_1 - W_o)}{W_2} \times 100 \quad (2)$$

$$Percent\ homopolymer\ (\%H) = 100 - \%GE \quad (3)$$

where W_o is the dry weight of the fiber treated with ionic liquid, W_1 and W_2 are the dry weights of cellulose-grafted-PLA nanocomposite film and *L*-lactide monomer used in the reaction, respectively.

Fourier Transform Infrared Spectroscopy (FTIR)

Fourier transform infrared (FTIR) spectra were performed using an ATR-FTIR spectrophotometer (Spectrum 100, Perkin Elmer, USA). Spectra were acquired within 4000–600 cm^{-1} region, using 64 scans overlapped and 1 cm^{-1} resolution. The results of the spectra were normalized.

X-ray Diffraction (XRD)

The X-ray diffraction patterns of the nanocomposite films were recorded using an X-ray diffractometer (PANalytical X'Pert PRO MPD Alpha1 powder diffractometer in a Bragg–Brentano $\theta/2\theta$ geometry of 240 millimetres of radius). The samples were analysed at the radiation wavelength of 1.5406 Å and 45 kV to 40 mA with the scanning range of 2° to 60° (2θ). The crystallinity index (CI) was calculated according to the following Eq. (4) [35]:

$$CrI\ (\%) = \frac{(I_2 00 - I_a m)}{I_2 00} \times 100 \quad (4)$$

where $I_2 00$ is the intensity of the peak assigned to the (200) reflection of cellulose Iβ, which is typically in the range 2θ= 21–23°. $I_a m$ is the minimum in the intensity occurs at about $2\theta = 18°$ for noncrystalline cellulose. Scherrer's Eq. (5) was used for estimating the crystallite size:

$$D = \frac{K/\lambda}{\beta/cos\theta} \quad (5)$$

where K is the constant of 0.9, λ is the wavelength of the incident X-ray (0.154056 nm), β is the FWHM (Full width at half maximum) of the diffraction peak in radians, and θ is the is the diffraction angle for the (200) plane [36].

Structural Properties

The roughness of the samples was analysed using a tridimensional (3D) roughness stylus profilometer (WYKO NT

1100 series Optical Profiling System, Veeco, Plainview, NY, USA).

The surface and cross-section of obtained nanocomposite films were observed by means of FE-SEM (model JSM-7100F, JEOL, USA) using an accelerating voltage of 10 kV. Prior to characterization, the samples were coated with a thin conducting layer of graphite. An energy-dispersive X-ray spectroscopy (EDS) attached to the SEM was carried out to further identify and map the presence of ZnONP on the cellulose matrix.

The Thickness and Mechanical Properties

The thickness of nanocomposite films were measured through a micrometer (Frank-PTI digital 16502, Germany), according to ISO 534:2011. At least five random locations of each film sample was measured, and the mean value of these estimations was calculated as the film thickness.

The mechanical properties of different formulations were determined with an universal testing machine (JJ Lloyd instrument, model T5K) equipped with a 500 N load cell, and across-head speed of 50 mm/min. Film samples used in tests were cut into rectangular shape with 40 mm length and 10 mm width. Prior to mechanical testing, the films were conditioned for at least one week at 25 °C and under 50%RH. Mechanical parameters, i.e., tensile strength, elongation at break and Young's modulus, were obtained from five replicates for each film formulation directly from the resulting stress-strain curves.

Optical Properties

L^* (lightness), a^* (redness-greenness) and b^* (yellowness–blueness) as the color parameters were determined using a colorimeter (Technidyne, UK). A white plate was used as a standard for color measurement ($\check{} = 92.92$) and color parameters were calculated at three random positions on the surface of the film. The total color difference (ΔE) between each color value of the standard color plate and film sample was obtained according to this following Eq. (6):

$$\Delta E = \sqrt{(L^* - L)^2 + (a^* - a)^2 + (b^* - b)^2} \tag{6}$$

UV and visible light barrier properties of the films were determined using a UV–Visible spectrophotometer (Evolution 600, Thermo Scientific) by measuring the light transmittance at 280 nm (T280) and 660 nm (T660), respectively, as described by Ngo et al. [37]. Firstly the samples were cut into a rectangular strips (1 cm × 3 cm) and then directly placed into the test cell of the spectrophotometer. The air was selected as a reference. For each composition film, three samples were measured, and the average vaule × standard deviation was reported.

Barrier Properties

Air permeability was evaluated in accordance to the standard ISO 5636-3:2013, by the Bendtsen permeability tester (Chevron Co., USA) with 10 replicates.

The water vapor permeability (WVP) of the nanocomposite film was measured gravimetrically by the ASTM E96 standard method with slight modification. For the measurement, the samples first were conditioned to an environmental chamber using a humidity chamber (model FX 1077, Jeio Tech Co. Ltd., Ansan, Korea) controlled at 25 °C and under 50%RH with an air movement of 198 m/min. Then, the test films were mounted on glass cups which was filled with 3 g of calcium chloride ($CaCl_2$) salt and was sealed by hot glue stick and parafilm to avoid water vapor penetration. The entire set, after weighing, was placed at 25 × 2 °C and 98 × 2%RH by measuring the weight at intervals of 1 and 24 h for 80 h. In order to calculate water vapor transmission rate (WVTR) in (g m^{-2} . day^{-1}), the slope was obtained from a chart of weight gain vs. time using a simple linear regression method. By dividing the slope of each line by surface of sample exposed to water vapor, WVTR was determined, according to the following Eq. (7).

$$WVTR = \frac{(G/t)}{A} = \frac{slope}{test\ area} \tag{7}$$

Finally, the WVP of the sample was measured using the following Eq. (8) [38]:

$$WVP = \frac{WVTR}{P(R_1 - R_2)} \times X \tag{8}$$

where X was the film thickness (m), P was the saturation vapour pressure of water at 25 °C (Pa), R1 is the relative humidity in the chamber (98%RH), and R2 is the relative humidity in the cups (0%RH).

Oxygen transmission rate (OTR) was measured using the apparatus MOCON OX-TRAN® Model 1/50, USA. The test consists in determining the amount of atmospheric oxygen concentration of 100% that passes through the surface (50 cm^2) of the film, in 24 h. The OTR tests were performed at two different conditions, 23 °C, 0%RH and 38 °C, 90%RH.

Water Contact Angle

The hydrophobicity was measured by the water contact angle (WCA). Contact angle of the nanocomposite films were carried out with a WCA analyzer (OCA15EC, Dataphysics Co., USA) using an image capture ratio of 25 frame/s. Film stripes

were prepared with a dimension of 1 cm × 5 cm and a drop of distilled water (approximately 5 µL) was placed on the surface of the sample using a micro-syringe. The contact angle was determined within 0–30 s and the digital images was taken after 0 s. At least five samples were performed for each formulation.

Antioxidant Activity

The antioxidant activity of nanocomposite film sample was determined using 2, 2′-azinobis-(3-ethylbenzothiazoline-6-sulfonic acid) ($ABTS^+$) radical scavenging activity method according to Valls et al. and Cusola et al. with modifications [39, 40]. In this method, the free radical scavenging activity was assessed by a spectroscopic method based on the disappearance of absorption band at 752 nm of the free radical $ABTS^+$. To summarize, the $ABTS^+$ solution was obtained by oxidation of potassium persulfate. The solution was diluted to obtain an absorbance of 0.70 × 0.1 at 752 nm. For comparison, 10 mg of the nanocomposite film samples were added to 1.5 mL of $ABTS^+$ solution and vortexed about 2 min. Afterwards, the samples were centrifuged 4 min at 6000 rpm. Finally, the samples were kept at room temperature in the dark for 30 min and measured the absorbance at 752 nm. The absorbance of film-free control sample was also taken at 752 nm in the same procedure. The analysis of antioxidant activity was performed at least 3 times for each sample. The antioxidant activity of the nanocomposite film was calculated according to the following Eq. (9):

$$Antioxidant\ activity\ (\%) = \frac{(A_o - A_1)}{A_o} \times 100 \quad (9)$$

where A_o was the absorbance of control (without sample) and A_1 was the absorbance of nanocomposite film sample.

Results and Discussion

Degree of Polymerization (DP) of Cellulose

Figure 2 shows the average DP of the cotton linter pulp, ACC and nanocomposite films. DP was 2297 for the original pulp and but decreased to 847 after partial dissolution (ACC). This result is consistent with previously reported data of Duchemin et al. [41]. Also, DP for the nanocomposite films, which were obtained by adding LA monomers and ZnONPs to a cellulose matrix, was higher than in ACC (1875 vs 1102). The increased DP observed may have resulted from the increased proportion of noncellulose components (PLA and ZnONPs) in the nanocomposite films increasing their viscosity.

Grafting Parameters

The concentration of *L*-lactide monomer in the reaction medium, as expected, had significant effects on grafting parameters. As shown in Table 1, the grafting percentage grew dramatically with increasing LA, maximum grafting (28.2%) was obtained at 70% LA in the nanocomposite film with 1% ZnONPs. The percentage of grafting increased to 36.6% when ZnONPs concentration was increased further (by 5%). An increase in grafting percentage was seen because the grafting process was catalyzed by the greater ZnONPs concentration, which is consistent with the results of Kaur et al. [31] and Rodriguez et al. [32]. In general,

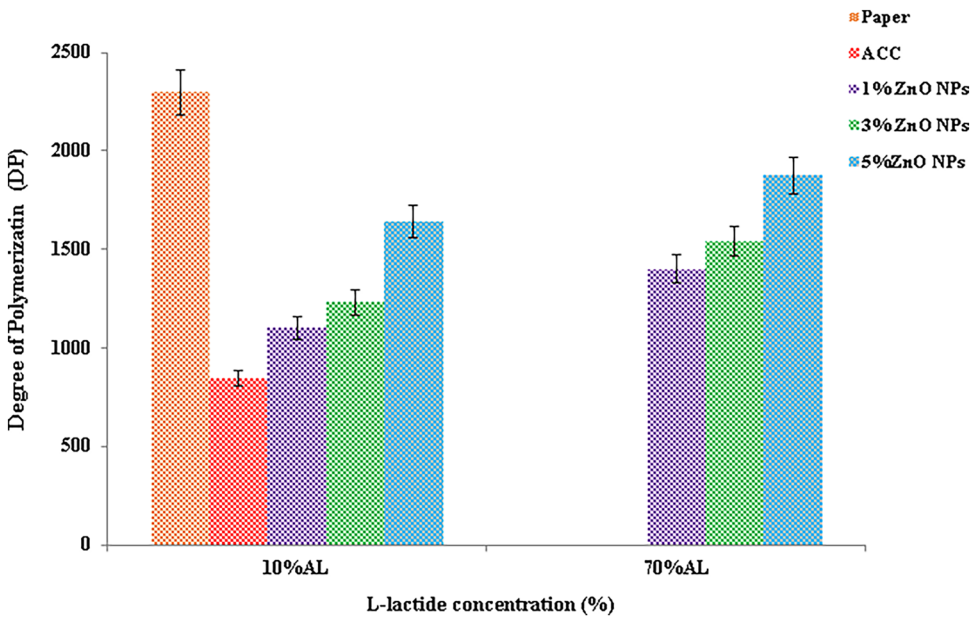

Fig. 2 Average degree of cellulose polymerization in pulp, ACC, cellulose-grafted-PLA nanocomposite films with different contents in ZnO nanoparticles and LA monomers

Table 1 %Grafting, %Grafting efficiency and %Homopolymer

Sample	Grafting (%)	Grafting efficiency (%)	Homopolymer (%)
1% ZnONPs/10% LA	1.54	16.66	83.33
1% ZnONPs/30% LA	7.72	27.03	72.3
1% ZnONPs/50% LA	18.14	38.21	61.78
1% ZnONPs/70% LA	28.18	41.95	58.04
3% ZnONPs/10% LA	2.70	29.16	70.83
3% ZnONPs/30% LA	9.65	33.78	66.21
3% ZnONPs/50% LA	23.55	49.6	50.40
3% ZnONPs/70% LA	34.74	51.72	48.27
5% ZnONPs/10% LA	3.47	36.4	64.2
5% ZnONPs/30% LA	13.51	47.1	52.05
5% ZnONPs/50% LA	26.25	55.73	44.26
5% ZnONPs/70% LA	36.67	55.88	44.11

the grafting efficiency depends on the LA concentration. The increase in monomer concentration resulted to increase in grafting efficiency. Low grafting efficiency means that less monomer was used in grafting and most was wasted in side reactions and homopolymer formation. In addition, the percentage of homopolymer showed a reverse trend with respect to grafting efficiency. This behavior can be attributed to accumulation of monomer at close proximity of the cellulose backbone [34, 42].

FTIR

Successful grafting of PLA onto the cellulose surface was confirmed by FTIR spectra recorded over the wavenumber range 4000–400 cm^{-1}. Figure 3 shows the spectra for cotton cellulose, ACC and the cellulose-grafted-PLA nanocomposite films obtained by using variable proportions of LA and ZnONPs. As can be seen, all spectra exhibited similar typical absorption bands; therefore, the catalysts (EmimAc and ZnONPs) had no influence on the chemical structure of cotton cellulose or regenerated cellulose in the dissolution and regeneration processes [43, 44]. The spectra for the nanocomposite films differed from that for cotton cellulose in three respects. Consistent with previous reports, the distinct peaks at 2923 and 2855 cm^{-1} were due to asymmetric and symmetric stretching of C–H bonds in methyl groups of grafted PLA chains [45, 46]. These bands increased with increasing content of LA and ZnONPs in the nanocomposite films.One other difference was the presence of a new absorption peak at 1750 cm^{-1} that was observed after in situ ROP of LA and corresponded to the carbonyl group (C=O) in PLA. No similar peak was present in the spectra for cotton cellulose or ACC film; also, its increased strength confirmed ROP of LA monomers with cellulose [18, 19]. Based on the normalized spectra, peak strength increased with increasing content of LA and ZnONPs in the regenerated cellulose matrix. This result suggests that the amount of PLA grafted from the surface can be adjusted through those of LA and ZnONPs added to the free initiator. The decreased strength of the typical bands for cellulose I at 1430 and 1110 cm^{-1} in ACC and the nanocomposite samples, which were strong in the spectrum for cotton cellulose, confirmed that some cellulose I was converted into cellulose II in the nanocomposite films [47, 48]. The bands at ca. 1565 and 1415 cm^{-1} were assigned red to stretching of the typical functional groups of EmimAc (C–N and C=N) which were absent from ACC

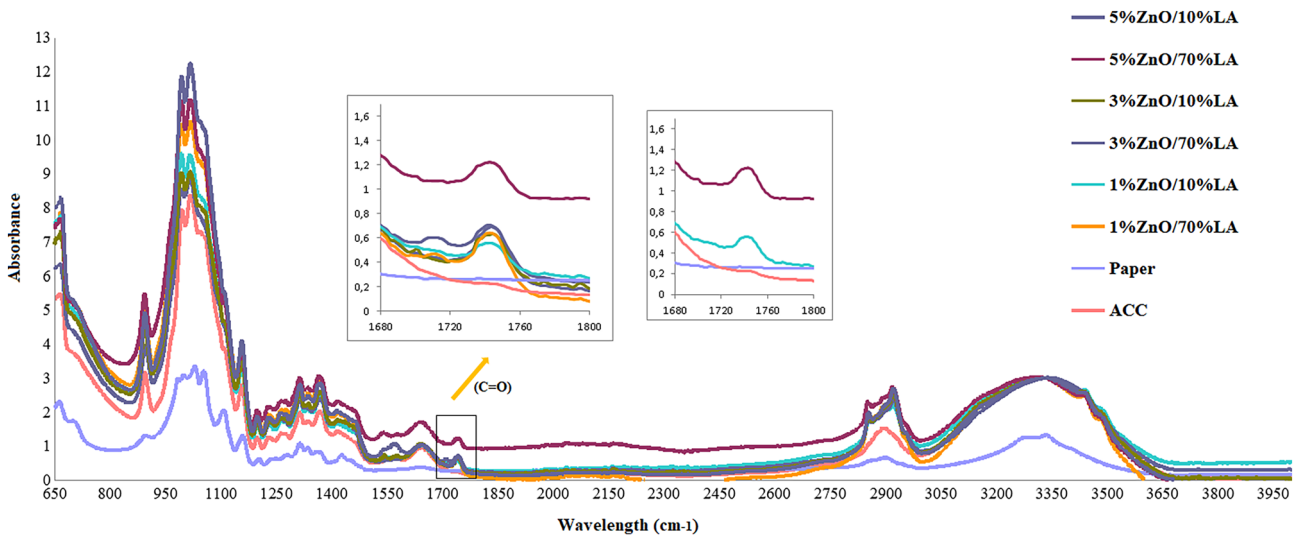

Fig. 3 FTIR spectra in the region from 4000 to 650 cm^{-1} for paper, ACC and cellulose-grafted PLA nanocomposite films with different contents in ZnO nanoparticles and LA monomers

and the nanocomposite films. This indicate that the washing step was effective to remove the majority of EmimAc from fibers [49, 50]. Finally, all samples exhibited a broad band at 3000–3650 cm^{-1} that was assigned to stretching of -OH groups and intermolecular or intramolecular hydrogen bonds in cellulose and adsorbed water [29, 51].

X-ray Diffraction Spectra

Crystallinity changes in cellulose upon PLA grafting were investigated by XRD spectroscopy. Figure 4a shows the XRD patterns for the starting cellulose, the regenerated cellulose film and the cellulose-grafted-PLA nanocomposite films with highest and lowest contents in LA and ZnONPs. Figure 4b shows the corresponding changes in crystalline index (CrI). The XRD spectrum for cotton linter cellulose exhibited well defined peaks for cellulose I at 2θ values of 14.8°, 16.6°, 22.8°, and 34.6° that were assigned to diffraction planes of $(\bar{1}10)$, (110), (200), and (004), respectively [7]. After partial dissolution and immersion in the coagulation bath, the diffraction pattern for the ACC film exhibited peaks at 2θ values of 12.2° $(\bar{1}10)$ and 20.7° (110), consistent with the crystalline form of cellulose II. The solvent treatment shifted the peak at $2\theta = 22.8°$ to the left and made it broader [52]. The crystalline index and crystallite size of cotton linter paper were 89.36% and 6.75 nm, respectively, and those of the ACC film 46.58% and 1.50 nm, respectively. The index of the original cellulose material was much higher than that of the ACC film, which suggests that partial dissolution with IL damaged or seriously altered the crystalline structure of cellulose fibers and increased the proportion of noncrystalline cellulose. The decrease in crystallite size from 6.75 to 1.50 nm additionally confirms that the solvent penetrated crystallites and dissolved amorphous sections, as well as outer chains in the crystallites. This result is consistent with others of Lu et al. [36]; Yousefi et al. [6]; Ghaderi et al. [52]. Grafting by PLA did not alter the typical XRD patterns for the nanocomposite films relative to the ACC film. Also, the crystalline index and crystallite size of both nanocomposite films were similar (ca. 52% and 1.46 nm, respectively). This result suggests that cellulose retained its original crystalline structure after grafting with further PLA and ZnONPs as reinforcing agents. In addition, according to the bibliography (Shankar et al. [53] and Asiri et al. [54]) ZnONPs should show diffraction peaks in the range of 30° and 40°. The reason why we did not detect these peaks could be that the ZnONPs are well integrated in the matrix and the XRD pattern of regenerated cellulose overlaps that of ZnO. On the other hand, as a result of ZnONPs incorporation into the regenerated film, the degree of crystallinity was slightly increased compared to the ACC film (from 46.58 to 56%). This increase in crystallinity was due to the crystalline nature of the Zn in ZnONPs as it has been reported by those of Zou et al. [55] and Gasti et al. [56].

Surface Morphology

The properties of the transparent nanocomposite film, and the surface micro- or nanostructures of the starting paper, ACC and nanocomposite films were examined by scanning electron microscopy (SEM). The spectra are shown at different magnifications in Figs. 5 and 6, and the average surface roughness (R_a) of the samples are shown in Fig. 7.

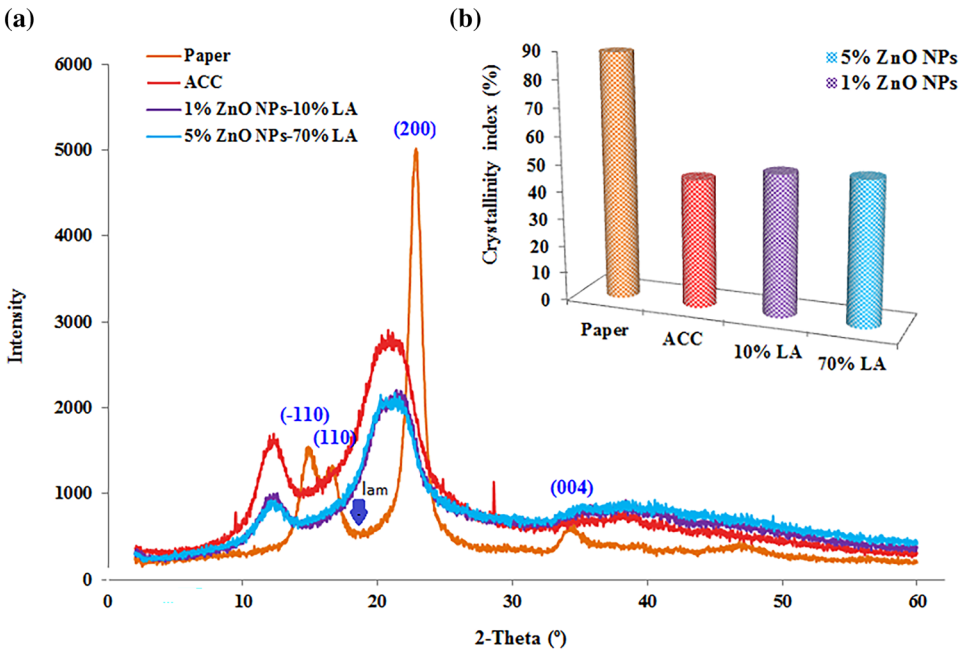

Fig. 4 XRD patterns of paper, ACC, cellulose-grafted-PLA nanocomposite films

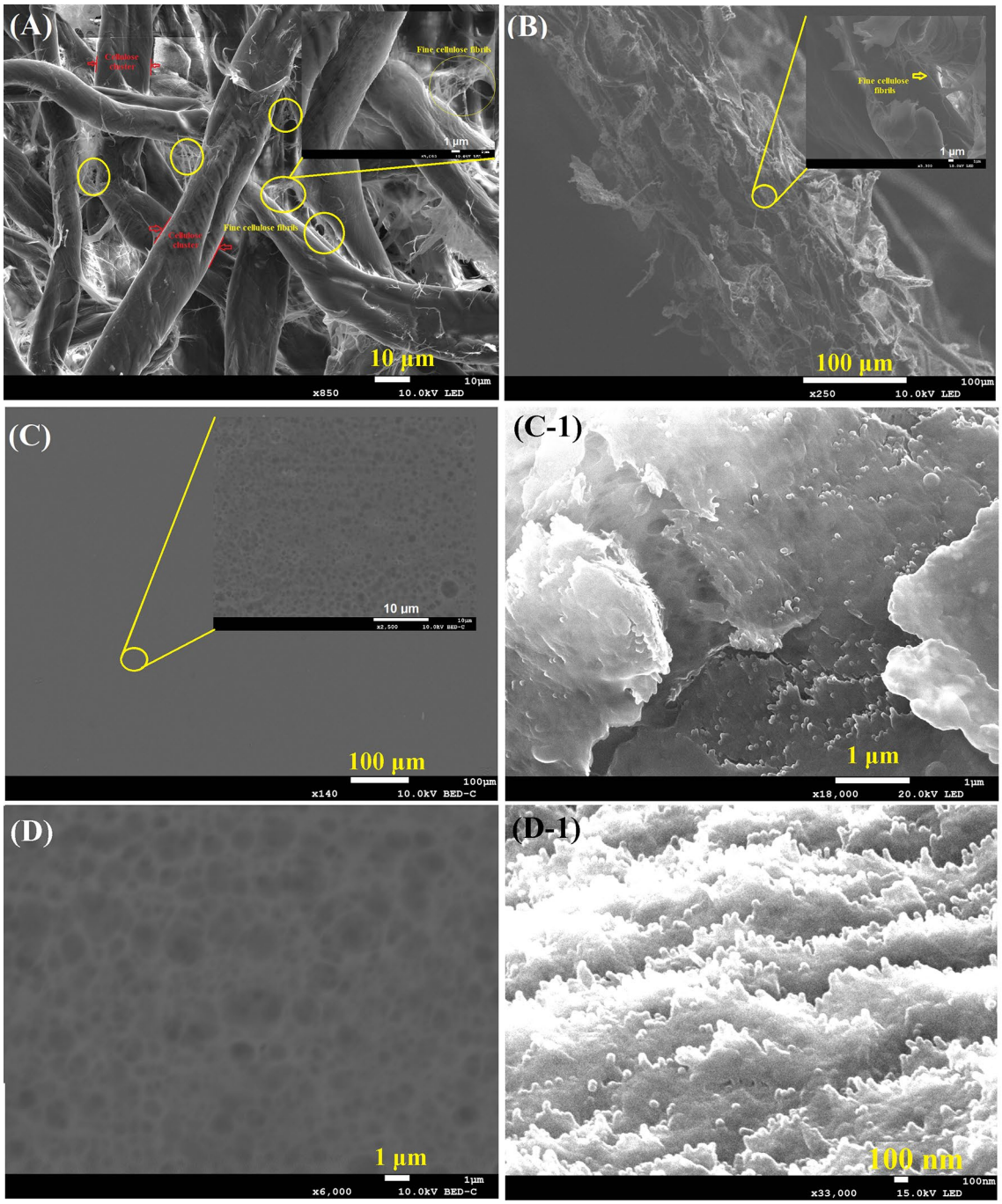

Fig. 5 SEM images at different magnifications illustrating the morphology of the surface and cross-section of paper (**A**, **B**) and ACC film (**C**, **D**)

As can be seen, unmodified cellulose paper exhibited a very open, porous network of crisscrossing fibers (Fig. 5a). There were many loosely composed micro- or nanosized pores between the crisscross cellulose clusters and fine fibrils (Fig. 5b). However, the porous, loose structures of unmodified cellulose paper became less apparent when the ionic liquid was added. As can be seen from the micrographs of Fig. 5c and d, IL facilitated partial dissolution of cellulose fibers, thereby leading to a smoother, more uniform, denser surface in the ACC film, which is consistent with the 3D roughness profilometry results. R_a for the ACC film was 8.5 nm (Fig. 7a). The results on the nanoscale also revealed that the welding agent successfully welded macro-, micro- and nanofibers to one other by penetrating deeply into the nano-gaps among nanofibrils (Fig. 5c-1 and d-1). Dissolution of the skin part of the nanofibril surfaces increased the

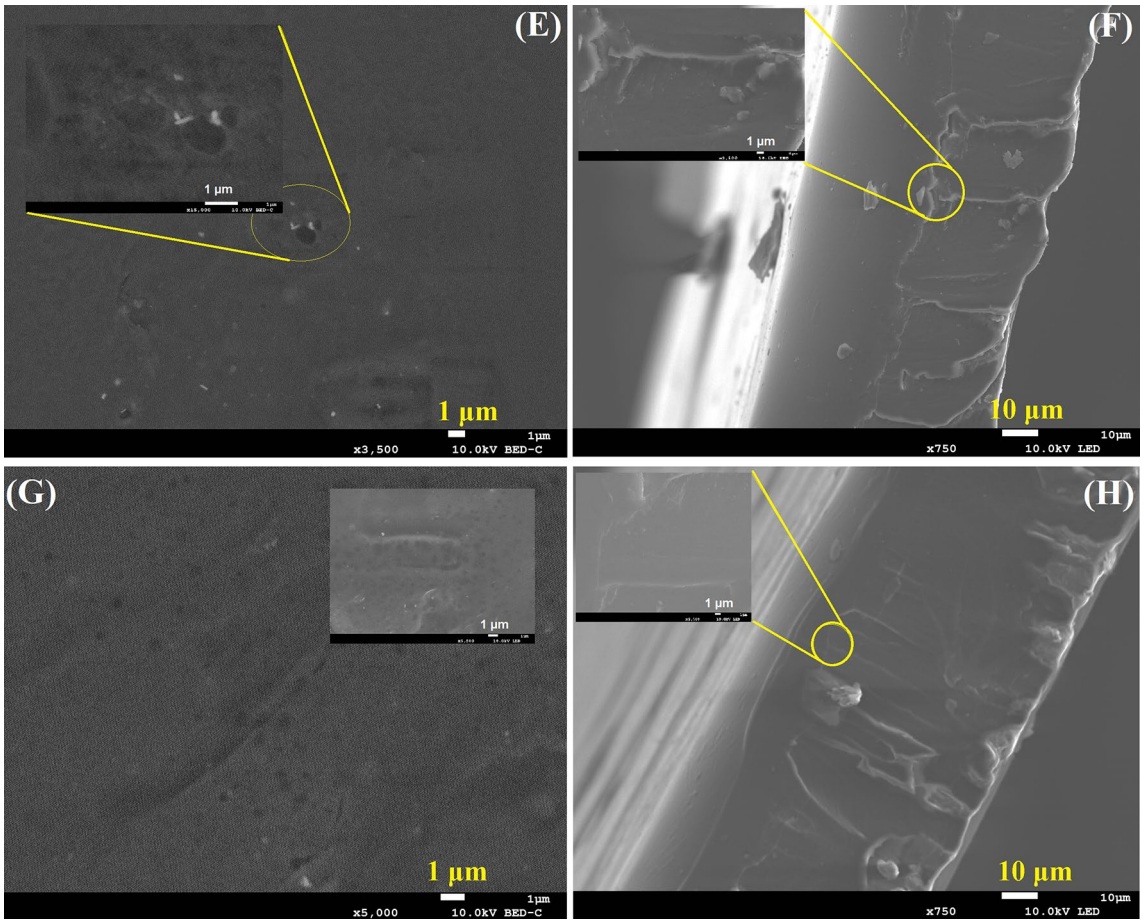

Fig. 6 SEM images at different magnifications illustrating the morphology of the surface and cross-section of a nanocomposite film containing 1% ZnONPs and 10% LA (**E**, **F**), and another containing 5% ZnONPs and 70% LA (**G**, **H**)

proportion of noncrystalline phase. This result indicates that ZnONPs penetrated nanopores or nanogapes among nanofibrils, which moved freely in the IL solvent. Regeneration and welding of nanostructures ensured trapping of nanoparticles with fully a consolidated structure. This result is consistent with those of Youseft et al. [6, 8] and Niu et al. [5].

Nanocomposites with the highest and lowest contents in PLA and ZnONPs were used to evaluate grafting and dispersion in regenerated cellulose. As can be seen fromFig. 6e, with small amounts of ZnONPs (1%) and LA (10%) regenerated cellulose exhibited a slightly rougher surface with few cavities and pores. The nanocomposite film was less smooth and uniform (roughness = 134.01 nm) than the ACC film (Fig. 7b).

The cross-sectional view of the film in (Fig. 6f) reveals a relatively homogeneous structure with good integration of the components in the polymer matrix. As can be seen in Fig. 6g and h, a compact surface morphology was also observed in the nanocomposite film obtained with a ZnONP loading of 5% and an LA loading of 70%. Clearly, increasing the two loadings decreased roughness and the number of cavities in the resulting film. This result is consistent with those of the profilometric analysis. R_a for this film and hence smaller than those for ACC and polyethylene terephthalate (7.0 nm; Fig. 7c).The decreased roughness of the film was likely due to the distribution of an increased proportion of PLA chains throughout the cellulose matrix.

EDS was used to analyze the components of a nanocomposite film obtained with 1%ZnONPs, and 10%LA. The Zn-associated peaks in the EDS spectra of Fig. 8b confirms the presence of Zn metal along with the C and O. Also, the spectrum of Fig. 8a testifies to the absence of elemental zinc from pure cotton paper.

Thickness and Mechanical Properties

Table 2 shows the thickness of cellulose-grafted-PLA nanocomposite films. IL welding reduced the thickness of the original paper (122 × 4.08 µm) to 48 × 2.05 µm in the ACC film as a result of the welding agent providing a more compact surface for macrofibers in the original paper. Also, thickness increased from 0.048 to 0.062 mm as the amounts

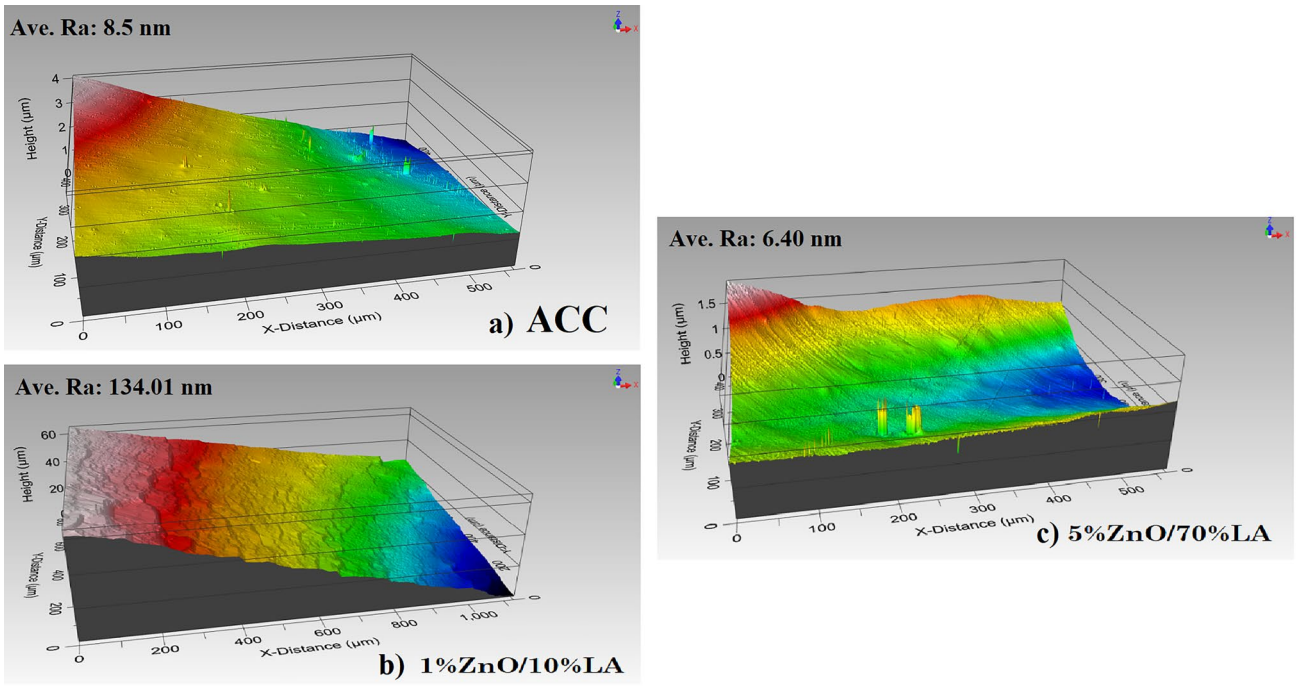

Fig. 7 Mean surface roughness of ACC and cellulose-grafted-PLA nanocomposite films with the lowest and highest contents in ZnONPs and LA monomers as acquired through from 3D profiles

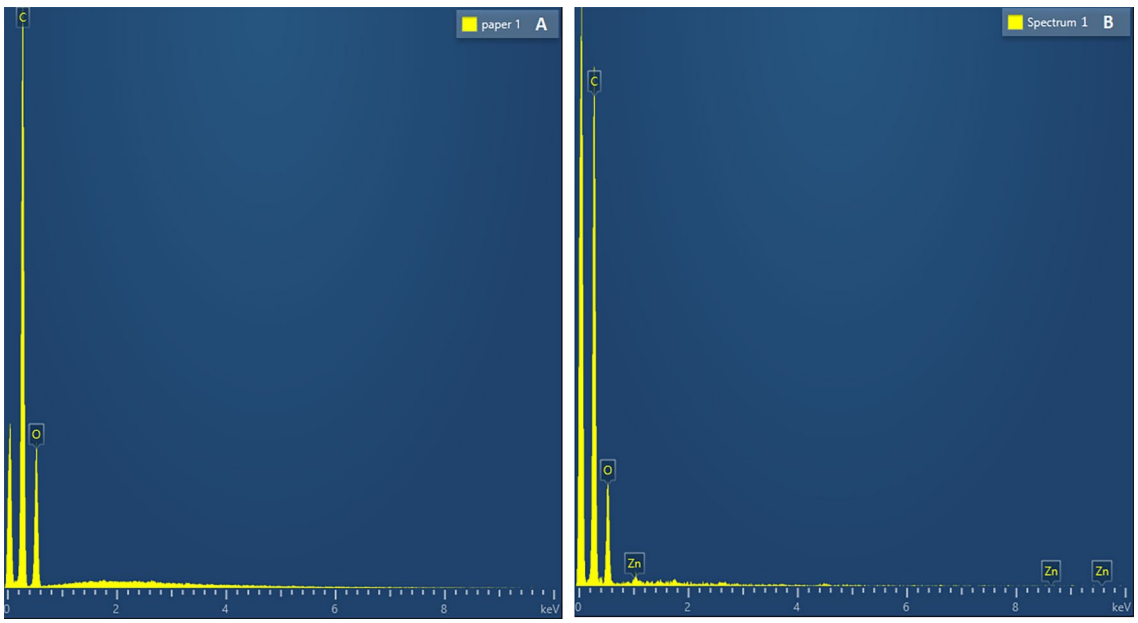

Fig. 8 EDS spectra for **A** untreated cotton paper and **B** a nanocomposite film containing 1%ZnONPs and 10%LA

of LA and ZnONPs added to the cellulose matrix were increased. Based on Table 1, the thickness of the nanocomposite film containing 5% ZnONPs and 70% LA differed little from that of the ACC film.

Figure 9 illustrates the mechanical properties of the cellulose-grafted-PLA nanocomposite films in terms of Young's modulus (YM), tensile strength (TS) and elongation at break (EB). These properties are especially important for food packaging films since poor flexibility and strength can lead to cracking during packaging and use. TS, EB and YM were 80.42 MPa, 16.61% and 19.13 GPa, respectively, for the ACC film; and 0.6 MPa, 3.17% and 0.19 GPa, respectively,

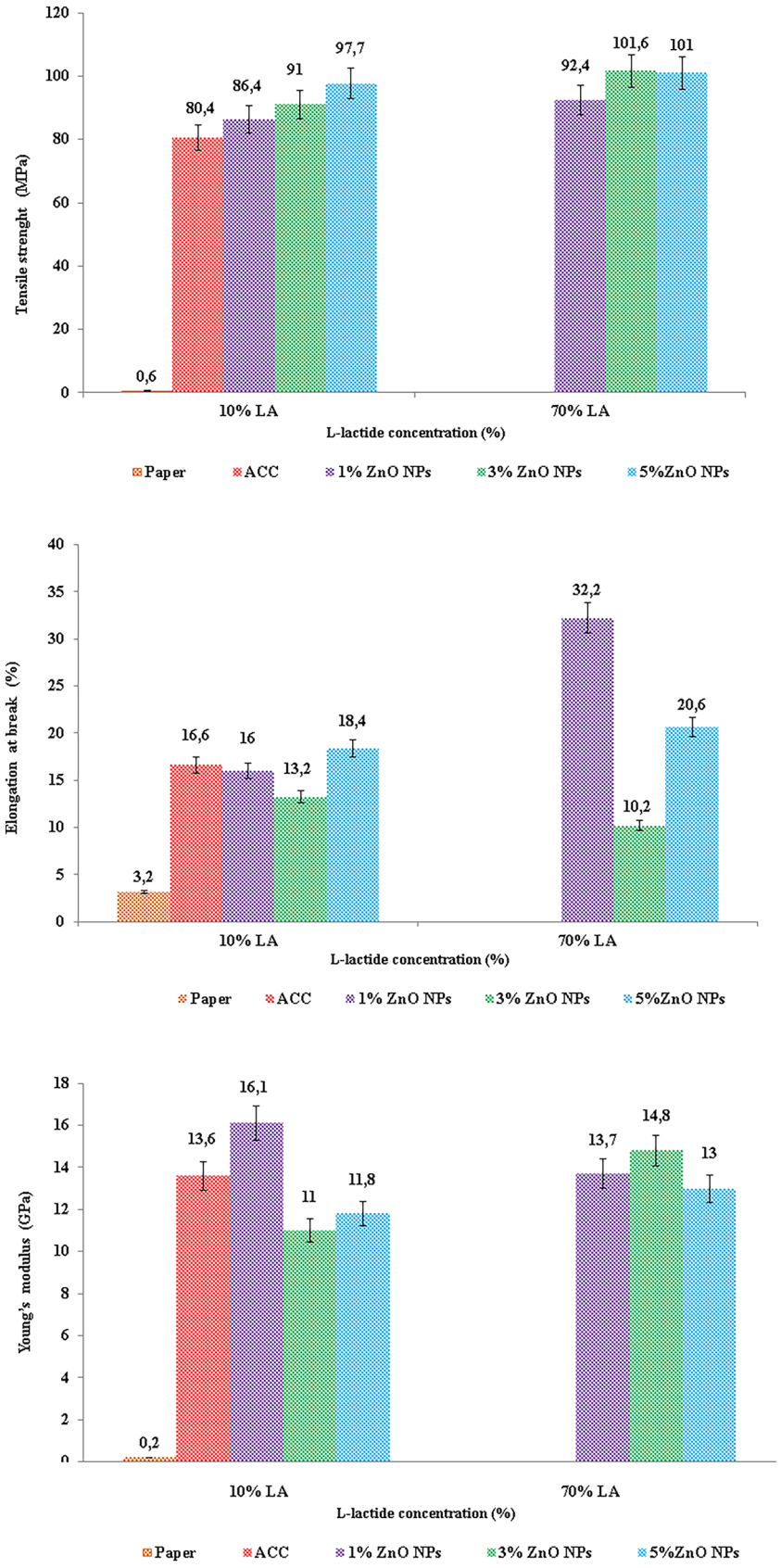

Fig. 9 **a** Tensile strength (MPa), **b** elongation at break (%) and **c** young's modulus (GPa) of paper, ACC and cellulose-grafted-PLA nanocomposite films with different contents in ZnO nanoparticles and LA monomers

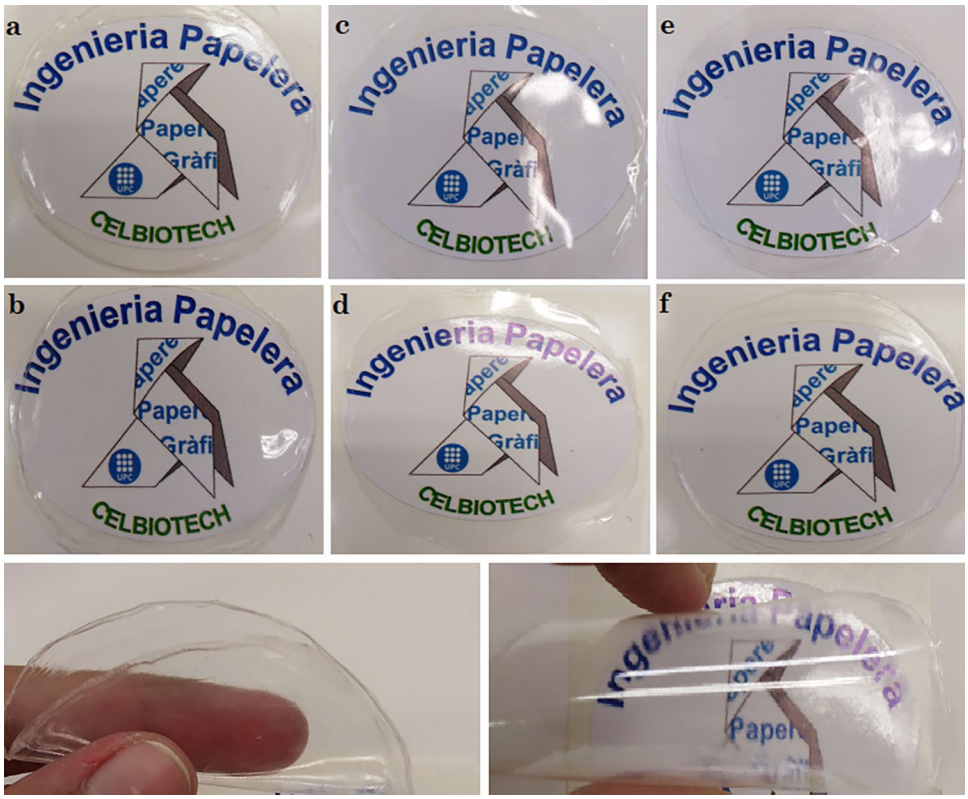

Fig. 10 Visual appearance, qualitative transparency and flexibility of cellulose-grafted-PLA nanocomposite films with variable contents in ZnONPs and LA. **a** 1%ZnONPs, 10%LA, **b** 1%ZnONPs, 70%LA, **c** 3%ZnONPs, 10%LA, **d** 3%ZnONPs, 70%LA, **e** 5%ZnONPs, 10%LA and **f** 5%ZnONPs, 70%LA

Table 2 Color, light transmittance (%) and thickness of various cellulose-grafted-PLA films

Sample	Color				Light transmittance (%)		Thickness (μm)
	L	a	b	Δ*E*	280 (nm)	660 (nm)	
ACC	88.75 × 0.05	− 1.32 × 0.03	3.25 × 0.05	4.24 × 0.15	81.90 × 0.76	85.42 × 0.42	48 × 2.05
1% ZnONPs/10% LA	89.90 × 0.34	− 1.30 × 0.004	3.18 × 0.04	3.10 × 0.33	63.07 × 0.42	83.89 × 0.49	49 × 1.24
1% ZnONPs/30% LA	89.15 × 0.36	− 1.27 × 0.01	3.48 × 0.04	3.91 × 0.15	64.17 × 2.83	81.16 × 0.67	53 × 2.05
1% ZnONPs/50% LA	89.77 × 0.14	− 1.26 × 0.1	3.37 × 0.21	3.37 × 0.19	63.91 × 3.34	81.82 × 1.27	56 × 1.63
1% ZnONPs/70% LA	89.60 × 0.16	− 1.27 × 0.01	3.22 × 0.07	3.41 × 0.06	63.38 × 0.22	82.86 × 0.32	61 × 1.24
3% ZnONPs/10% LA	89.99 × 0.11	− 1.29 × 0.04	3.25 × 0.03	3.26 × 0.02	47.82 × 037	84.77 × 2.05	52 × 1.00
3% ZnONPs/30% LA	89.29 × 0.12	− 1.29 × 0.04	3.41 × 0.22	3.76 × 0.18	40.25 × 1.28	83.09 × 1.96	55 × 2.05
3% ZnONPs/50% LA	89.69 × 0.76	− 1.27 × 0.005	3.21 × 0.65	3.31 × 0.12	38.24 × 0.75	77.05 × 1.55	58 × 1.24
3% ZnONPs/70% LA	89.59 × 0.14	− 1.26 × 0.01	3.20 × 0.05	3.40 × 0.19	35.89 × 0.09	79.09 × 1.61	62 × 0.94
5% ZnONPs/10% LA	88.43 × 0.37	− 1.24 × 0.02	3.49 × 0.04	4.60 × 0.63	30.59 × 0.34	82.00 × 2.36	55 × 1.63
5% ZnONPs/30% LA	88.33 × 0.08	− 1.22 × 0.03	3.84 × 0.04	4.80 × 0.25	28.79 × 092	79.80 × 2.68	57 × 0.81
5% ZnONPs/50% LA	88.84 × 0.63	− 1.25 × 0.02	3.46 × 0.12	4.20 × 0.18	25.02 × 1.14	73.93 × 2.79	58 × 0.47
5% ZnONPs/70% LA	88.87 × 0.02	− 1.29 × 0.07	3.31 × 0.21	4.13 × 0.28	23.08 × 0.35	73.68 × 1.82	62 × 1.24

for the cellulose-grafted PLA nanocomposite film. The increased mechanical strength of the ACC film (134-fold) can be ascribed to the IL welder penetrating deeply into nanogaps, lumens and pits by effect of microdisconnection and nanodisconnections between nanofibrils and of the increased connectivity and integrity of a network containing more junction points. This result is consistent with others of Ghaderi et al. [52], Yousefi et al. [8] and Niu et al. [5]. A plausible explanation for this softening effect and significant increase in ductility is that the cellulose bulk and surface were probably plasticized by EmimAc during the nanowelding process and became more flexible as a result [5, 57].

As can be seen from Fig. 9, adding ZnONPs to the regenerated cellulose matrix increased its mechanical strength. The tensile strength of the nanocomposite film was further enhanced with increase in LA content. No significant

difference in TS, EB or YM in the regenerated cellulose matrix was observed with the addition of 1%ZnONPs and 10%LA relative to the ACC film. However, the film exhibited a flexibility (EB) roughly twofold that of the control sample (ACC) on average with 70%LA added to the regenerated cellulose matrix. The increased EB value (30%) of the cellulose-grafted-PLA nanocomposite film suggests that a 1% proportion of ZnONPs was better dispersed and interacted more efficiently with PLA polymer chains and the regenerated cellulose matrix [5, 52]. Adding a 3% proportion of ZnONPs together with 70% LA to the regenerated cellulose matrix increased TS to 101.61 MPa but decreased EB to 24.78% by effect of the nanofillers restricting motion of the polymer chain. Interestingly, an LA proportion of 70% reduced EB to 20.58% with no change in TS or YM on increasing the proportion of ZnONPs from 3 to 5%. An increase in TS and a decrease in EB in nanocomposite films by effect of adding ZnONPs was previously observed by Shankar et al. [53] and Ngo et al. [37]. YM for the nanocomposite films containing 70% LA decreased with increase in the amount of ZnONPs added, albeit not significantly. TS, EB and YM for the film containing 5% ZnONPs and 70% LA were 101.05 MPa, 20.58% and 13.05 GPa, respectively, and suggest that the film was relatively strong and quite flexible. Therefore, using ZnONPs and LA in their optimum proportions ensured that film strength was improved to a similar extent.

Optical Properties

Figure 10 illustrates the appearance and flexibility of the cellulose-grafted-PLA nanocomposite films. As can be seen, all were adequately transparent and flexible. Transparent packaging is seemingly more attractive than are opaque food containers to store fresh foods because, consumers can easily check their freshness [58].

The color of the cellulose-grafted-PLA nanocomposite films is important for their acceptance as food packaging . Table 2 shows the lightness (L^*), and parameters a^* (green-red), b^* (blue-yellow) and ΔE(total color difference), for the films. As can be seen, neither a^* nor b^* differed significantly with the proportion of ZnONPs over the range 1-5%. The nanocomposite films containing 1% or 3% ZnONPs and variable proportions of LA had similar L^* values (89.15 to 89.99). However, a proportion of ZnONPs of 5% slightly decreased L^* with no effect on a^* or b^*. The decrease in L^* resulted in an increase in ΔE. Thus, ΔE for the nanocomposite films containing 1% and 3% of ZnONPs was 3.91 and 3.76, but rose to 4.80 with 5% of ZnONPs. A similar decreasing trend in L^* and increasing trend in ΔE with addition of ZnONPs to PLA and cellulose based films was previously found elsewhere [59].

Transmission of UV and visible light by the cellulose-grafted-PLA nanocomposite films were determined at 280 and 660 nm, respectively (Table 2). Compared to the ACC film, incorporating of ZnO nanoparticles into the regenerated cellulose matrix considerably decreased UV transmittance, which is in consistent with previous results of Saedi et al. [58]. The films containing 1% ZnONPs were ineffective in blocking UV light, which is unsurprising given their high transmittance of visible light at 660 nm (81–83%). However, increasing the proportion of ZnONPs from 3% to 5% in the films containing 70% LA dramatically reduced with 70%LA resulted in a dramatic reduction in UV transmittance (to 35.89% and 23.08%, respectively) with no appreciable impact on visible light transmittance. Therefore, incorporating ZnONP into regenerated cellulose improved its UV barrier properties with little loss of transparency, and hence made it acceptable for food packaging. Also, seemingly, UV light absorption increased with increasing film thickness, which confirms that the thickness of polymer films is a key factor in enhancing their UV shielding properties.

Barrier Properties

Air permeability measurements (0 μm $Pa^{-1}\,s^{-1}$) revealed that all nanocomposites and the ACC film, like the polyethylene and polypropylene packaging polymers used as controls, were completely impermeable to air. Therefore, the welding process provided an integrated, dense structure that formed a highly efficient air barrier [6].

Moisture transfer across packaging materials can have a strong impact on the shelf-life of packaged products. Water vapor permeability (WVP) has frequently been used to assess film barrier properties. In a nanocomposite film, WVP depends on the nature of its constituent polymers, its thickness and molecular weight, and the type of cross-linking agent used and its concentration [60, 61]. Figure 11 shows WVP for the nanocomposite films and the control samples (viz., untreated paper, and ACC and PLA films). WVP for the ACC film was approximately 45% lower than it was for untreated paper (15.70×10^{-9} g m^{-1} h^{-1} Pa^{-1}) but similar to that for PLA film.

This result confirms that welding process improved the barrier properties of the films [50]. A similar decrease in WVP was observed in the cellulose-grafted-PLA films enriched with the addition of either ZnONPs or in situ ROP of LA monomers. Obviously, ZnONPs acted synergistically with PLA; thus, the nanocomposite containing 5%ZnONPs and 70%LA had a WVP 82.35% lower than that of the ACC film. This makes cellulose-grafted-PLA nanocomposite films highly promising materials for food packaging. The reduction in WVP was a result of the hydrophobicity of ZnONPs and PLA added to the cellulose matrix [46, 62].

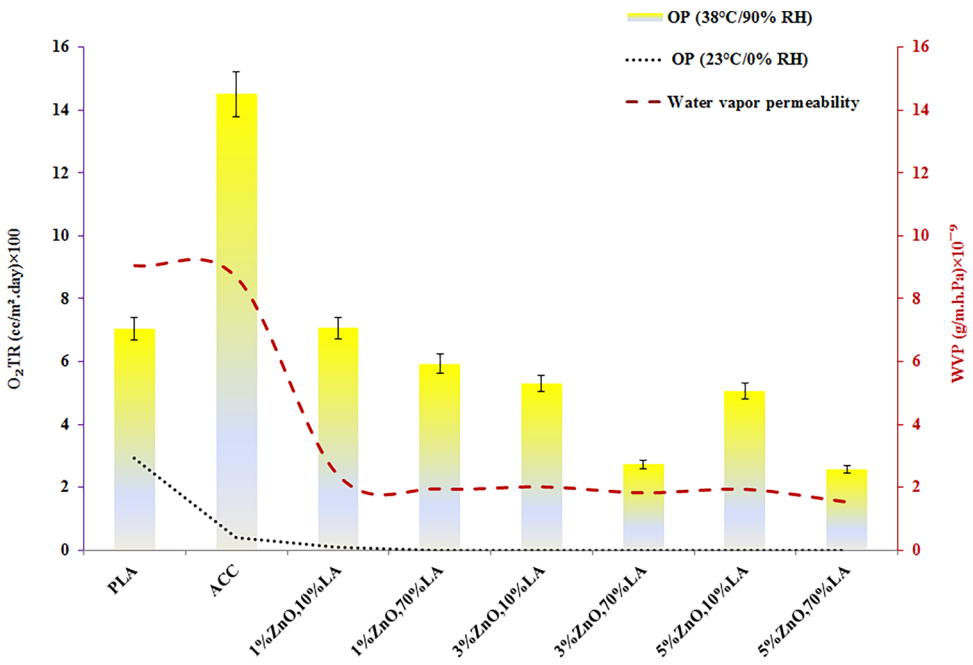

Fig. 11 OTR and WVP of paper, ACC and cellulose-grafted-PLA nanocomposite films with different contents in ZnO nanoparticles and LA monomers

Because oxygen is one of the main cause of food spoilage by effect of lipid oxidation and increased microbial growth, packaging materials should have good oxygen barrier properties [58]. As can be seen in Fig. 11, the OTR values at 0% and 90% RH of the nanocomposites were lower than those of the ACC and PLA films used as controls.

The OTR decreased with increasing proportion of ZnONPs and LA in the regenerated cellulose matrix. At 0% RH, the films were completely impermeable to oxygen. However, their permeability increased as RH was risen to 90%. This was a result of cellulose swelling and its matrix cracking to an increasing extent with increasing relative humidity [63]. At 90% RH, increasing proportion of LA to 70% with 5%ZnONPs decreased OTR by 65% relative to the nanocomposite film containing 1% ZnONPs,and 10%LA. Based on the results, the presence of increased amounts of ZnONPs and PLA polymers chains in the cellulose matrix can create tortuous pathways for oxygen to diffuse [61, 64].

Good oxygen barrier properties are important for many uses, including for food packaging. However, no particular barrier rating scales have to date been established. Abdellatief et al. [65] classified films as 'high oxygen barrier', 'medium oxygen barrier' and 'low oxygen barrier' according to whether their approximate OTR values at 23 °C, 50%RH fell in the range 1–10, 10–1000 and 1000–10,000 cc m^{-2} day^{-1}, respectively. At present, the most widely used commercial food packaging materials are made of polyethylene terephthalate (PET), which has an OTR value of around 110 cc m^{-2} day^{-1}. Based on this understanding, and on the low OTR values of the nanocomposite films, they could be used as packaging materials for food and pharmaceuticalsin tablet form (blisters), fresh meat, peanuts, and instant coffee, which are required to have OTR values lower than 100, 80, 50, and 2 cc m^{-2} day^{-1}, respectively (Gao et al. [66]; Wang et al. [67]; Markus et al. [68]).

Water Contact Angle

Surface hydrophobicity or hydrophilicity in films is usually measured in terms of water contact angle (WCA).

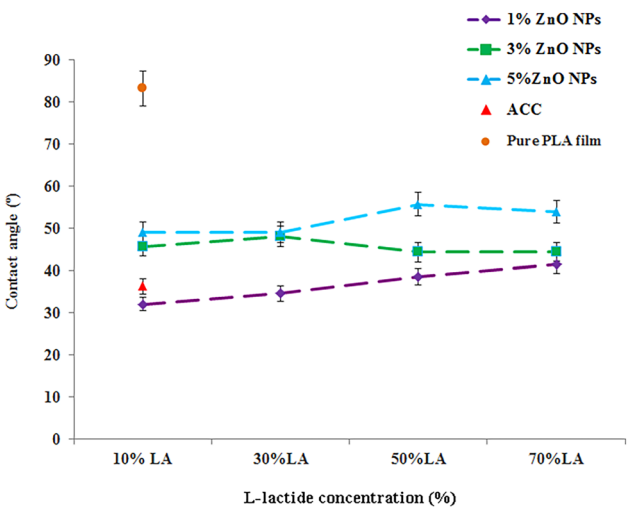

Fig. 12 Water contact angle of paper, ACC and cellulose-grafted-PLA nanocomposite films with different contents in ZnO nanoparticles and LA monomers

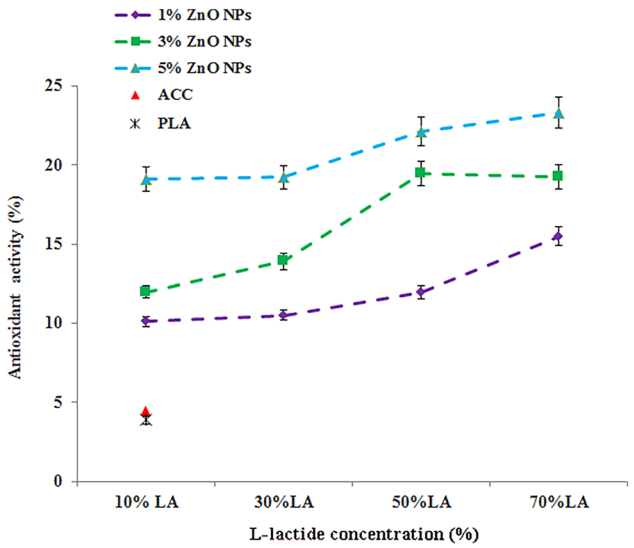

Fig. 13 Antioxidant activity of paper, ACC and cellulose-grafted-PLA nanocomposite films with different contents in ZnO nanoparticles and LA monomers

Hydrophobicity and hydrophilicity can be influenced by various factors including surface chemistry and roughness [69]. As can be seen from the WCA values of Fig. 12, all nanocomposite films were hydrophilic. Their decreased values relative to the PLA film were a result of the presence of hydroxyl groups in the nanocomposites. However, blending of LA monomers to the cellulose matrix decreased wettability and increased WCA. Thus, WCA for the film containing 1% ZnONPs and 70% LA was greater than that for the film containing 1%ZnONPs, 10%LA (41.49° vs 32.18°). Whereas increasing the proportion LA had little effect on WCA, increasing that of ZnONPs increased it substantially (from 34.64° in the nanocomposite film containing 1% ZnONPs and 30% LA to 44.38° and 55.78° in those containing 3 and 5 wt% ZnONPs, respectively). These results are suggestive of a positive relationship between WCA and the ZnONP loading [37, 70]. The decreased WCA value of the film containing 1%ZnONPs and 10% or 30%LA relative to the ACC film may have resulted from an increased surface roughness [70]. WCA for the film containing 5% ZnONPs and 10% LA was 49.04° but increased to 55.78° and 53.94° with 50% and 70% LA, respectively.

Antioxidant Activity

Antioxidant properties are especially important owing to the detrimental action of free radicals on foods and biological systems [71].Antioxidant activity in the cellulose-grafted-PLA nanocomposite films was assessed by ABTS radical scavenging. As can be seen from Fig. 13, the ACC film exhibited little activity through reaction of exposed electron-donating hydroxyl groups in the cellulose matrix with free radicals over time [72]. The addition of ZnONPs in increasing proportions substantially increased antioxidant activity in the films, however. According to Ananthalakshmi et al. [73], ZnONPs are among the best candidates for boosting antioxidant activity [73]. The films containing 1%ZnONPs and either 10%LA or 30%LA exhibited a similar activity (approximately 10%). This was also the case with those containing 5% ZnONPs and either 10% or 30% LA (ca. 19%). The highest antioxidant activity (23%) was that of the film containing 5%ZnONPs and 70%LA. By contrast, the pure PLA film exhibited insubstantial activity (<5%), probably because it acted as a reservoir and protector for ZnONPs in the film matrix. Overall, cellulose-grafted-PLA nanocomposite films containing ZnONPs can be used in active packaging to extend the shelf life of foods.

Conclusions

In this work, we developed a novel approach to preparing cellulose-grafted-PLA nanocomposite films from cellulose fibers by use of IL and simultaneous in situ ring-opening polymerization (ROP) of LA monomers with entrapped ZnO nanoparticles. As shown by SEM, the films had a relatively smooth, uniform structure. Based on the result, the ionic liquid facilitated mutual welding of fibers and micro- and nanofibrils by penetrating deeply into the nanogaps between nanofibrils. Based on XRD spectra, the welding agent altered the crystalline structure of cellulose fibers and increased their proportion of noncrystalline areas. Grafting PLA and adding ZnO nanoparticles (ZnONPs) modified the physical and functional properties of the films in relation to an all-cellulose composite (ACC). Thus, incorporating a 70% proportion of monomeric LA and one of 5% of ZnONPs improved some film properties including antioxidant activity and water contact angle. Increased proportions of ZnONPs and LA led to excellent barrier properties against UV and visible light, water vapor permeability and oxygen transmission rate. By contrast, the addition of ZnONPs or LA had no significant influence on color or light transmission. Increased proportions of LA (70%) and decreased proportions of ZnONPs (1%) improved the flexibility of the nanocomposite films in terms of elongation at break (up to 32%), whereas a proportion of 5% ZnONPs and one of 70% of LA maximized tensile strength. The resulting nanocomposite films have the potential for a variety of uses.

Acknowledgements This research received financial support from the PID2020-114070RB-I00 (CELLECOPROD) project [MCIN/AEI/10.13039/ 501100011033]. The first author, E. Amini, gratefully acknowledges the Universitat Politècnica de Catalunya and Banco Santander for the financial support of her predoctoral grant FPI-UPC.

Author Contributions All authors contributed to the study conception and design. Material preparation, data collection and analysis were performed by EA. The first draft of the manuscript was written by EA and all authors commented on previous versions of the manuscript. All authors read and approved the final manuscript.

Funding Open Access funding provided thanks to the CRUE-CSIC agreement with Springer Nature. The authors declare that no funds were received during the preparation of this manuscript.

Declarations

Conflict of interest The authors declare that they have no known competing financial interests or personal relationships that could have influenced the work reported in this paper.

References

1. Islam MU, Khan S, Ullah MW, Park JK (2017) Recent advances in biopolymer composites for environmental issues. In: Thakur VK, Thakur MK, Kessler MR (eds) Handbook of composites from renewable materials. Scrivener publishing llc, Beverly, pp 673–691
2. Hua S, Chen F, Liu ZY, Yang W, Yang MB (2016) Preparation of cellulose-graft-polylactic acid via melt copolycondensation for use in polylactic acid based composites: synthesis, characterization and properties. RSC Adv 6(3):1973–1983
3. Ryu MH, Park J, Oh DX, Hwang SY, Jeon H, Im SS et al (2017) Precisely controlled two-step synthesis of cellulose-graft-poly (L-lactide) copolymers: effects of graft chain length on thermal behavior. Polym Degrad Stab 142:226–233
4. Roy D, Semsarilar M, Guthrie JT, Perrier S (2009) Cellulose modification by polymer grafting: a review. Chem Soc Rev 38(7):2046–2064
5. Niu X, Liu Y, King AW, Hietala S, Pan H, Rojas OJ (2019) Plasticized cellulosic films by partial esterification and welding in low-concentration ionic liquid electrolyte. Biomacromolecules 20(5):2105–2114
6. Yousefi H, Mashkour M, Yousefi R (2015) Direct solvent nanowelding of cellulose fibers to make all-cellulose nanocomposite. Cellulose 22(2):1189–1200
7. Niu X, Huan S, Li H, Pan H, Rojas OJ (2021) Transparent films by ionic liquid welding of cellulose nanofibers and polylactide: enhanced biodegradability in marine environments. J Hazard Mater 402:124073
8. Yousefi H, Nishino T, Faezipour M, Ebrahimi G, Shakeri A (2011) Direct fabrication of all-cellulose nanocomposite from cellulose microfibers using ionic liquid-based nanowelding. Biomacromolecules 12(11):4080–4085
9. Guzman-Puyol S, Ceseracciu L, Tedeschi G, Marras S, Scarpellini A, Benítez JJ et al (2019) Transparent and robust all-cellulose nanocomposite packaging materials prepared in a mixture of trifluoroacetic acid and trifluoroacetic anhydride. Nanomaterials 9(3):368
10. Amini E, Valls C, Roncero MB (2021) Ionic liquid-assisted bioconversion of lignocellulosic biomass for the development of value-added products. J Clean Prod 326:129275
11. Vijayakrishna K, Manojkumar K, Sivaramakrishna A (2015) Ionic liquids as solvents and/or catalysts in polymerization. In: Mecerreyes D (ed) Applications of ionic liquids in polymer science and technology. Springer, Cham, pp 355–387
12. Vinogradova YS, Chen JY (2016) Micron-and nano-cellulose fiber regenerated from ionic liquids. J Textile Inst 107(4):472–476
13. Kosan B, Michels C, Meister F (2008) Dissolution and forming of cellulose with ionic liquids. Cellulose 15(1):59–66
14. Cusola O, Valls C, Vidal T, Tzanov T, Roncero MB (2015) Electrochemical insights on the hydrophobicity of cellulose substrates imparted by enzymatically oxidized gallates with increasing alkyl chain length. ACS Appl Mater Interfaces 7(25):13834–13841
15. Zhang X, Liu C, Zhang A, Sun R (2018) Synergistic effects of graft polymerization and polymer blending on the flexibility of xylan-based films. Carbohydr Polym 181:1128–1135
16. Jiang F, Pan C, Zhang Y, Fang Y (2019) Cellulose graft copolymers toward strong thermoplastic elastomers via RAFT polymerization. Appl Surf Sci 480:162–171
17. Terzopoulou Z, Baciu D, Gounari E, Steriotis T, Charalambopoulou G, Bikiaris D (2018) Biocompatible nanobioglass reinforced poly (ε-caprolactone) composites synthesized via in situ ring opening polymerization. Polymers 10(4):381
18. Khaw YY, Chee CY, Gan SN, Singh R, Ghazali NNN, Liu NS (2019) Poly (lactic acid) composite films reinforced with microcrystalline cellulose and keratin from chicken feather fiber in 1-butyl-3-methylimidazolium chloride. J Appl Polym Sci 136(24):47642
19. Wang X, Jia Y, Liu Z, Miao J (2018) Influence of the lignin content on the properties of poly (lactic acid)/lignin-containing cellulose nanofibrils composite films. Polymers 10(9):1013
20. Somord K, Suwantong O, Tawichai N, Peijs T, Soykeabkaew N (2016) Self-reinforced poly (lactic acid) nanocomposites of high toughness. Polymer 103:347–352
21. Dong F, Yan M, Jin C, Li S (2017) Characterization of type-II acetylated cellulose nanocrystals with various degree of substitution and its compatibility in PLA films. Polymers 9(8):346
22. Zhang X, Chen M, Liu C, Zhang A, Sun R (2015) Homogeneous ring opening graft polymerization of caprolactone onto xylan in dual polar aprotic solvents. Carbohydr Polym 117:701–709
23. Carlmark A, Larsson E, Malmström E (2012) Grafting of cellulose by ring-opening polymerisation-a review. Eur Polym J 48(10):1646–1659
24. Hafrén J, Córdova A (2005) Direct organocatalytic polymerization from cellulose fibers. Macromol Rapid Commun 26(2):82–86
25. Hafrén J, Córdova A (2007) Direct Bronsted acid-catalyzed derivatization of cellulose with poly (L-lactic acid) and D-mandelic acid. Nordic Pulp Paper Res J 22(2):184–187
26. Yan C, Lv Y, Yu J, Wu J, Zhang J, Zhang J et al (2009) Thermoplastic cellulose-graft-poly (L-lactide) copolymers homogeneously synthesized in an ionic liquid with 4-dimethylaminopyridine catalyst. Biomacromolecules 10(8):2013–2018
27. Dong H, Xu Q, Li Y, Mo S, Cai S, Liu L (2008) The synthesis of biodegradable graft copolymer cellulose-graft-poly (L-lactide) and the study of its controlled drug release. Colloids Surf B 66(1):26–33
28. Farooq A, Patoary MK, Zhang M, Mussana H, Li M, Naeem MA et al (2020) Cellulose from sources to nanocellulose and an

overview of synthesis and properties of nanocellulose/zinc oxide nanocomposite materials. Int J Biol Macromol 154:1050–1073
29. Roy S, Rhim JW (2020) Carboxymethyl cellulose-based antioxidant and antimicrobial active packaging film incorporated with curcumin and zinc oxide. Int J Biol Macromol 148:666–676
30. Zhang X, Luo W, Xiao N, Chen M, Liu C (2020) Construction of functional composite films originating from hemicellulose reinforced with poly (vinyl alcohol) and nano-ZnO. Cellulose 27(3):1341–1355
31. Kaur H, Rathore A, Raju S (2014) A study on ZnO nanoparticles catalyzed ring opening polymerization of L-lactide. J Polym Res 21(9):1–10
32. Rodríguez-Tobías H, Morales G, Enríquez-Medrano FJ, Grande D (2017) Performance of zinc oxide nanoparticles as polymerization initiating systems in the microwave-assisted synthesis of poly (d, l-lactide)/ZnO nanocomposites. Macromol Symp 374:1600102
33. Aditya A, Chattopadhyay S, Jha D, Gautam HK, Maiti S, Ganguli M (2018) Zinc oxide nanoparticles dispersed in ionic liquids show high antimicrobial efficacy to skin-specific bacteria. ACS Appl Mater Interfaces 10(18):15401–15411
34. Villocillo C, Angcajas A (2019) Biosorption of copper(II) ions in aqueous solution by microwave-synthesized starch-graft-N-methyl-N-vinylacetamide. Biosci Biotechnol Res Commun 12:211–221
35. Segal L, Creely JJ, Martin A Jr, Conrad C (1959) An empirical method for estimating the degree of crystallinity of native cellulose using the X-ray diffractometer. Text Res J 29(10):786–794
36. Lu P, Cheng F, Ou Y, Lin M, Su L, Chen S et al (2017) Rapid fabrication of transparent film directly from wood fibers with microwave-assisted ionic liquids technology. Carbohydr Polym 174:330–336
37. Ngo TMP, Dang TMQ, Tran TX, Rachtanapun P (2018) Effects of zinc oxide nanoparticles on the properties of pectin/alginate edible films. Int J Polym Sci 2018:1–9
38. Babaee M, Garavand F, Rehman A, Jafarazadeh S, Amini E, Cacciotti I (2022) Biodegradability, physical, mechanical and antimicrobial attributes of starch nanocomposites containing chitosan nanoparticles. Int J Biol Macromol 195:49–58
39. Valls C, Roncero MB (2013) Antioxidant property of TCF pulp with a high hexenuronic acid (HexA) content. Holzforschung 67(3):257–263
40. Cusola O, Valls C, Vidal T, Roncero MB (2015) Conferring antioxidant capacity to cellulose based materials by using enzymatically-modified products. Cellulose 22(4):2375–2390
41. Duchemin BJ, Mathew AP, Oksman K (2009) All-cellulose composites by partial dissolution in the ionic liquid 1-butyl-3-methylimidazolium chloride. Composite A 40(12):2031–2037
42. Sand A, Yadav M, Behari K (2010) Synthesis and characterization of alginate-g-vinyl sulfonic acid with a potassium peroxydiphosphate/thiourea system. J Appl Polym Sci 118(6):3685–3694
43. Dissanayake N, Thalangamaarachchige VD, Troxell S, Quitevis EL, Abidi N (2018) Substituent effects on cellulose dissolution in imidazolium-based ionic liquids. Cellulose 25(12):6887–6900
44. Kim I, Viswanathan K, Kasi G, Sadeghi K, Thanakkasaranee S, Seo J (2019) Poly (lactic acid)/ZnO bionanocomposite films with positively charged ZnO as potential antimicrobial food packaging materials. Polymers 11(9):1427
45. Lin N, Chen G, Huang J, Dufresne A, Chang PR (2009) Effects of polymer-grafted natural nanocrystals on the structure and mechanical properties of poly (lactic acid): a case of cellulose whisker-graft-polycaprolactone. J Appl Polym Sci 113(5):3417–3425
46. Miao C, Hamad WY (2016) In-situ polymerized cellulose nanocrystals (CNC)-poly (l-lactide)(PLLA) nanomaterials and applications in nanocomposite processing. Carbohydr Polym 153:549–558
47. Cao Y, Li H, Zhang Y, Zhang J, He J (2010) Structure and properties of novel regenerated cellulose films prepared from cornhusk cellulose in room temperature ionic liquids. J Appl Polym Sci 116(1):547–554
48. Pang J, Wu M, Zhang Q, Tan X, Xu F, Zhang X et al (2015) Comparison of physical properties of regenerated cellulose films fabricated with different cellulose feedstocks in ionic liquid. Carbohydr Polym 121:71–78
49. Chen P, Xie F, Tang F, McNally T (2020) Ionic liquid (1-ethyl-3-methylimidazolium acetate) plasticization of chitosan-based bionanocomposites. ACS Omega 5(30):19070–19081
50. Reyes G, Borghei M, King AW, Lahti J, Rojas OJ (2018) Solvent welding and imprinting cellulose nanofiber films using ionic liquids. Biomacromolecules 20(1):502–514
51. Xie Q, Wang S, Chen X, Zhou Y, Fang H, Li X et al (2018) Thermal stability and crystallization behavior of cellulose nanocrystals and their poly (l-lactide) nanocomposites: effects of surface ionic group and poly (d-lactide) grafting. Cellulose 25(12):6847–6862
52. Ghaderi M, Mousavi M, Yousefi H, Labbafi M (2014) All-cellulose nanocomposite film made from bagasse cellulose nanofibers for food packaging application. Carbohydr Polym 104:59–65
53. Shankar S, Wang LF, Rhim JW (2018) Incorporation of zinc oxide nanoparticles improved the mechanical, water vapor barrier, UV-light barrier, and antibacterial properties of PLA-based nanocomposite films. Mater Sci Eng C 93:289–298
54. Asiri AM, Petrosino F, Pugliese V, Khan SB, Alamry KA, Alfifi SY et al (2021) Synthesis and characterization of blended cellulose acetate membranes. Polymers 14(1):4
55. Zou Z, Ismail BB, Zhang X, Yang Z, Liu D, Guo M (2023) Improving barrier and antibacterial properties of chitosan composite films by incorporating lignin nanoparticles and acylated soy protein isolate nanogel. Food Hydrocolloids 134:108091
56. Gasti T, Dixit S, Hiremani VD, Chougale RB, Masti SP, Vootla SK et al (2022) Chitosan/pullulan based films incorporated with clove essential oil loaded chitosan-ZnO hybrid nanoparticles for active food packaging. Carbohydr Polym 277:118866
57. Liu P, Guo X, Nan F, Duan Y, Zhang J (2017) Modifying mechanical, optical properties and thermal processability of iridescent cellulose nanocrystal films using ionic liquid. ACS Appl Mater Interfaces 9(3):3085–3092
58. Saedi S, Shokri M, Kim JT, Shin GH (2021) Semi-transparent regenerated cellulose/ZnONP nanocomposite film as a potential antimicrobial food packaging material. J Food Eng 307:110665
59. Zhang R, Lan W, Ji T, Sameen DE, Ahmed S, Qin W et al (2021) Development of polylactic acid/ZnO composite membranes prepared by ultrasonication and electrospinning for food packaging. LWT 135:110072
60. Taghizadeh M, Mohammadifar MA, Sadeghi E, Rouhi M, Mohammadi R, Askari F et al (2018) Photosensitizer-induced cross-linking: a novel approach for improvement of physicochemical and structural properties of gelatin edible films. Food Res Int 112:90–97
61. Wu J, Sun Q, Huang H, Duan Y, Xiao G, Le T (2019) Enhanced physico-mechanical, barrier and antifungal properties of soy protein isolate film by incorporating both plant-sourced cinnamaldehyde and facile synthesized zinc oxide nanosheets. Colloids Surf B 180:31–38
62. Li W, Li L, Cao Y, Lan T, Chen H, Qin Y (2017) Effects of PLA film incorporated with ZnO nanoparticle on the quality attributes of fresh-cut apple. Nanomaterials 7(8):207
63. Koppolu R, Lahti J, Abitbol T, Swerin A, Kuusipalo J, Toivakka M (2019) Continuous processing of nanocellulose and polylactic acid into multilayer barrier coatings. ACS Appl Mater Interfaces 11(12):11920–11927
64. Ahmed J, Arfat YA, Al-Attar H, Auras R, Ejaz M (2017) Rheological, structural, ultraviolet protection and oxygen barrier

properties of linear low-density polyethylene films reinforced with zinc oxide (ZnO) nanoparticles. Food Packag Shelf Life 13:20–26
65. Abdellatief A, Welt BA (2013) Comparison of new dynamic accumulation method for measuring oxygen transmission rate of packaging against the steady-state method described by ASTM D3985. Packag Technol Sci 26(5):281–288
66. Gao Q, Lei M, Zhou K, Liu X, Wang S, Li H (2020) Preparation of a microfibrillated cellulose/chitosan/polypyrrole film for Active Food Packaging. Prog Org Coat 149:105907
67. Wang J, Gardner DJ, Stark NM, Bousfield DW, Tajvidi M, Cai Z (2018) Moisture and oxygen barrier properties of cellulose nanomaterial-based films. ACS Sustain Chem Eng 6(1):49–70
68. Markus S, Kerstin D, Elodie B, Dario C, Florian W, Lazzeri A et al (2012) Properties of whey-protein-coated films and laminates as novel recyclable food packaging materials with excellent barrier properties. Int J Polym Sci. https://doi.org/10.1155/2012/562381
69. Fernández-Santos J, Valls C, Cusola O, Roncero MB (2022) Composites of cellulose nanocrystals in combination with either cellulose nanofibril or carboxymethylcellulose as functional packaging films. Int J Biol Macromol 211:218–229
70. Noshirvani N, Ghanbarzadeh B, Mokarram RR, Hashemi M, Coma V (2017) Preparation and characterization of active emulsified films based on chitosan-carboxymethyl cellulose containing zinc oxide nano particles. Int J Biol Macromol 99:530–538
71. Lukic I, Vulic J, Ivanovic J (2020) Antioxidant activity of PLA/PCL films loaded with thymol and/or carvacrol using scCO2 for active food packaging. Food Packag Shelf Life 26:100578
72. Priyadarshi R, Kim SM, Rhim JW (2021) Carboxymethyl cellulose-based multifunctional film combined with zinc oxide nanoparticles and grape seed extract for the preservation of high-fat meat products. Sustain Mater Technol 29:e00325
73. Ananthalakshmi R, Rajarathinam S, Sadiq AM (2019) Antioxidant activity of ZnO Nanoparticles synthesized using Luffa acutangula peel extract. Res J Pharm Technol 12(4):1569–1572